united nations
educational, scientific
and cultural
organization

international atomic
energy agency

the
abdus salam
international centre for theoretical physics

ICTP 40th Anniversary

SCHOOL ON SYNCHROTRON RADIATION AND APPLICATIONS
In memory of J.C. Fuggle & L. Fonda

19 April - 21 May 2004

Miramare - Trieste, Italy

1561/28

GISAXS, GID and X-Ray Reflectivity in Materials Science

S. Bernstorff

strada costiera, 11 - 34014 trieste italy - tel. +39 040 2240111 fax +39 040 224163 - sci_info@ictp.trieste.it - www.ictp.trieste.it

GISAXS, GID and X-Ray Reflectivity in Materials Science

S. Bernstorff
Sincrotrone Trieste
Strada Statale 14, km 163.5, in Area Science Park
34012 Basovizza / Trieste, Italy

ICTP School on Synchrotron Radiation and Applications
19 Apr - 21 May 2004

Why X-ray scattering with grazing incidence in materials science?

In the opto-electonic industry, the goal is to fabricate devices of allways maller dimensions, with novel structures / features, etc. Nanostructures in implanted semiconductors, or on thin wafers (Si, GaAs with nanometer sized islands from Ge, InAs on it), offer technologically interesting applications: if nanocrystals have dimensions of the de Boglie wavelength of the electron, energy levels become quantisized, and correspondingly e.g. sharp photoluminescence lines are found. Such "quantum dot" systems are promising candidates for novel device applications like optoelectronic switches, photodiodes, lasers, etc.
For adequate performance, a macroscopic number of quantum dots with a high degree of structural homogeneity is needed. Since opto-electronic properties of quantum dots depend mainly on strain, size, size distribution and ordering, it becomes essential to characterize these quantities as a function of the growth parameters. Furthermore, a precise control of growth parameters such as substrate temperature, deposition rate and substrate miscut is necessary to grow coherently strained small islands with remarkable structural and optoelectronic properties.

Work in this direction has been done using e.g. atomic force microscopy. With it a large variety of different shapes has been found (e.g. faceted pyramids, hut clusters, dome-like structures, …).

Disadvantage:
- Small sampling statistics -> size distribution and ordering effects can hardly be discovered
- Strain cannot be detected
- Buried dots are not accessible

X-ray scattering:
- Averages over macroscopic areas, but still yields microscopic information
- Is intrinsically sensitive to strain
- In case of grazing incidence techniques, structural information can be obtained with depth resolution.

Conventional large angle X-ray scattering methods: the signal from a single quantum dot layer on a substrate is typically 10^{-6} times weaker than the scattering from the substrate. This intensity ratio can be improved if grazing incidence techniques are applied: the penetration depth of X-rays can be restricted to about 10 nm, thus probing only the sample volume in which the quantum dots occur. Since the absolute number of atoms in the dots is small, the use of highly brilliant synchrotron sources is mandatory for these techniques.

X-ray scattering by surfaces and interfaces

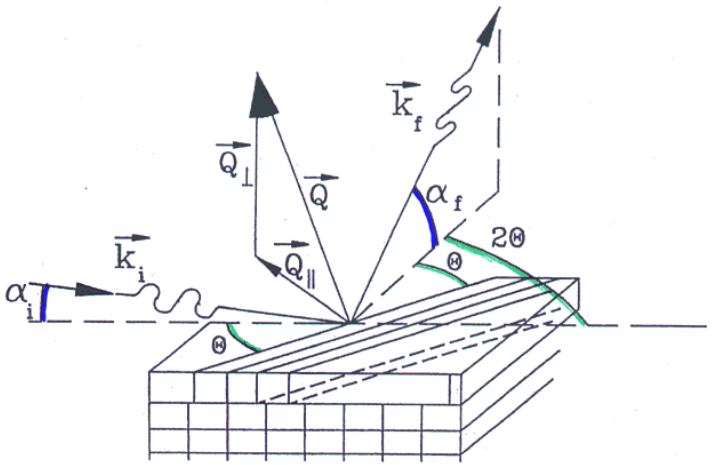

Grazing incidence X-ray scattering geometry: identical to 3D-case, except that

- incident beam (wavevector $\vec{k}_i$) is kept at glancing incidence angle α_i with respect to the surface
- scattered beam (wavevector $\vec{k}_f$) is detected at α_f with respect to sample surface, and at an angle 2Θ with respect to the transmitted beam direction.

Momentum transfer $\vec{Q} = \vec{k}_f - \vec{k}_i$ is often decomposed (relative to the surface) into 2 components $\vec{Q}_\parallel$ and $\vec{Q}_\perp$

$Q_\perp = k(\sin\alpha_i + \sin\alpha_f)$ with $k = \frac{2\pi}{\lambda}$

λ = wavelength

When α_i and α_f very small:

- $\vec{Q} \approx \vec{Q}_{ll}$
- scattering plane nearly ll to surface
- diffracting net planes nearly $\perp$ to surface

Scattering geometry : defined by directions of incident beam and detector direct

to reach diffraction condition:

rotate sample about its surface normal so that netplanes make $\measuredangle \theta$ with respect to both incident and scattered beam

↓

probe long-range periodicity parallel to sample surface

to see reflected beam: $\alpha_i = \alpha_f$

$2\theta = 0$

Refraction of X-rays at grazing angles

α_i is small → effects of refraction at the surface need to be considered

refractive index n of matter for X-rays:

$$\boxed{n = 1 - \delta + i\beta}$$

with:

$$\delta = \frac{1}{2\pi} \frac{e^2}{mc^2} \frac{N_a \Sigma_i (Z_i - f_i')}{\Sigma_i A_i} \rho \lambda^2$$

$$= 2.701 \times 10^{-6} \frac{\Sigma_i (Z_i - f_i') \text{ [el. units]}}{\Sigma_i A_i \text{ [g/mol]}} \rho \text{[g/cm}^3\text{]} \lambda^2 \text{[Å]}$$

$$\beta = \frac{1}{2\pi} \frac{e^2}{mc^2} \frac{N_a \Sigma_i f_i''}{\Sigma_i A_i} \rho \lambda^2 = \mu \frac{\lambda}{4\pi}$$

with: N_a Avogradro's number

Summation over all atomic species i

$(Z_i - f_i')$ scattering factor

f_i'' anomalous dispersion factor

A_i atomic weight

} of the i species

ρ density

λ wave length

μ photo electric absorption coefficient

typical orders of magnitude:

$\delta \sim 10^{-5}$

$\beta \sim 10^{-6}$

$\alpha_c \sim \sqrt{2\delta} \sim 0.1° - 0.5°$ (critical angle)

e.g. for 10keV photons:

element	Z	δ	β	α_c (deg)
C (diamond)	6	4.6×10^{-6}	4.5×10^{-9}	0.173
Si	14	4.9×10^{-6}	7.4×10^{-8}	0.180
Cu	29	1.6×10^{-5}	1.9×10^{-6}	0.326
Au	79	3.0×10^{-5}	2.2×10^{-6}	0.443

Note

- real part of $n = 1 - \delta + i\beta$ is always slightly < 1
- because of refraction, a beam coming from vacuum into a sample comes closer to the sample surface
- for $\alpha_i < \alpha_c$, the beam is totally reflected, and only an evanescent wave, which decays over tens of angstroms, is present below the surface
- for $\alpha_i > \alpha_c$ the transmitted wave propagates

Scattering Depth

The perpendicular components of the incident and emergent wave vectors are modified upon crossing the surface, and become complex due to refraction and absorption:

$$k'_{i,f,\perp} = \frac{2\pi}{\lambda}\left(A_{i,f} - i B_{i,f}\right)$$

For small incidence and emergence angles:

$$A_{i,f} = \frac{1}{\sqrt{2}}\left(\sqrt{\left(\alpha_{i,f}^2 - \alpha_c^2\right)^2 + 4\beta^2} + \alpha_{i,f}^2 - \alpha_c^2\right)^{1/2}$$

$$B_{i,f} = \frac{1}{\sqrt{2}}\left(\sqrt{\left(\alpha_{i,f}^2 - \alpha_c^2\right)^2 + 4\beta^2} + \alpha_c^2 - \alpha_{i,f}^2\right)^{1/2}$$

→ the perpendicular momentum transfer inside the sample $Q'_\perp = k'_{f\perp} - k'_{i\perp}$ becomes complex.

The scattering depth

$$\Lambda = \frac{1}{\mathrm{Im}(Q'_\perp)} = \frac{\lambda}{4\pi\,(B_i + B_f)}$$

is thus strongly affected by refraction when α_i or α_f are close to α_c.

Scattering Depth

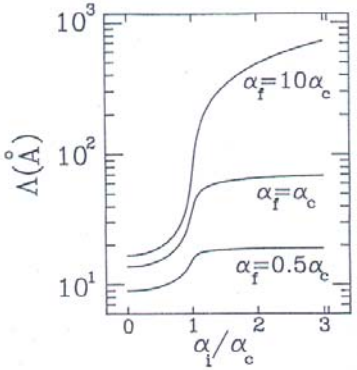

Pt surface
1.5 Å = λ

Variation of the scattering depth as a function of the incidence angle, for three exit angles, equal to half, one time and n times the critical angle, for a Pt surface and 1.5 Å wavelength.

Transmission coefficient

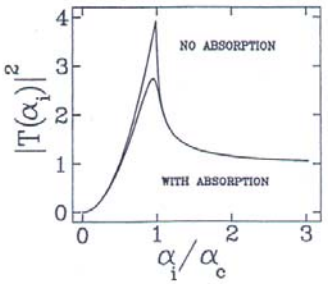

Intensity transmission coefficient for a Pt surface and 1.5 Å wavelength, with and without considering absorption.

The reflection and transmission coefficients are also strongly affected by refraction:

$$R_{i,f} = \frac{\alpha_{i,f}^2 - 2\alpha_{i,f}A_{i,f} + A_{i,f}^2 + B_{i,f}^2}{\alpha_{i,f}^2 + 2\alpha_{i,f}A_{i,f} + A_{i,f}^2 + B_{i,f}^2}$$

$$T_{i,f} = \frac{4\alpha_{i,f}^2}{\alpha_{i,f}^2 + 2\alpha_{i,f}A_{i,f} + A_{i,f}^2 + B_{i,f}^2}$$

$R_{i,f} = 1$ for $\alpha_{i,f} < \alpha_c$ (regime of total external reflection)

$T = 4$ (max. value) at α_c → fix α_i and/or α_f at α_c to enhance surface scattering!

II-VI semi-conductors Nanostructures : what for ?

quantum confinement of excitons, increase of the energy gap

↓

- **variable length optical absorbers**
- **high-speed non-linear optical switches**
- **photoluminiscence with variabel wavelength by changing particle size (-> quantum dot laser)**
- **formation of nanoparticles in dielectrics and non-absorbing materials**

BUT: working devices will depend on a precise control of size and density of an ensemble of Quantum Dots (QD)

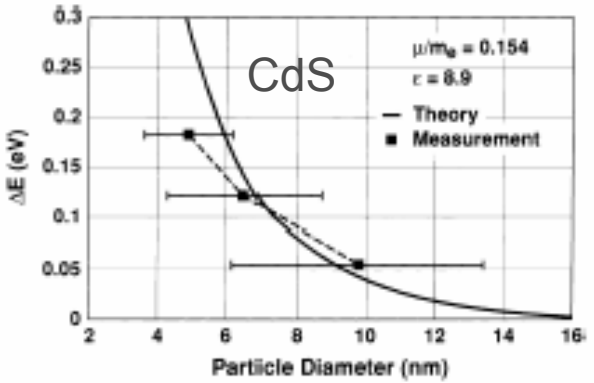

Fig. 5. Calculated and measured bandgap shift for CdS nanocrystals. The solid line is calculated from Eq. (2). The points are measurements of the bandgap shift from Eq. (1) for the samples in Fig. 4.

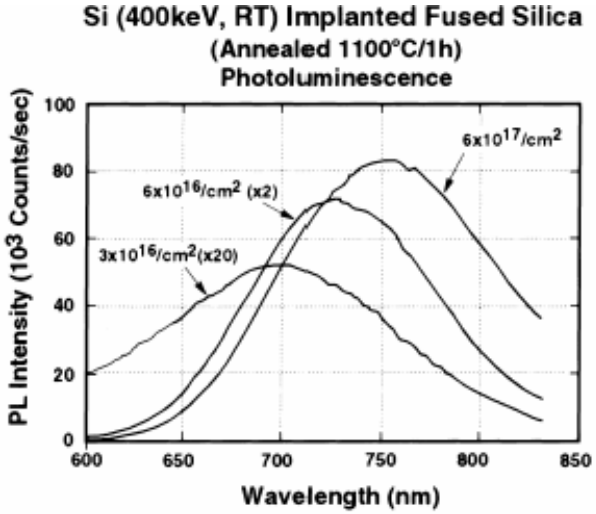

C.W. White et al. / Nucl. Instr. and Meth. in Phys. Res. B 141 (1998) 228

Schematic of the ion implantation technique for NC production

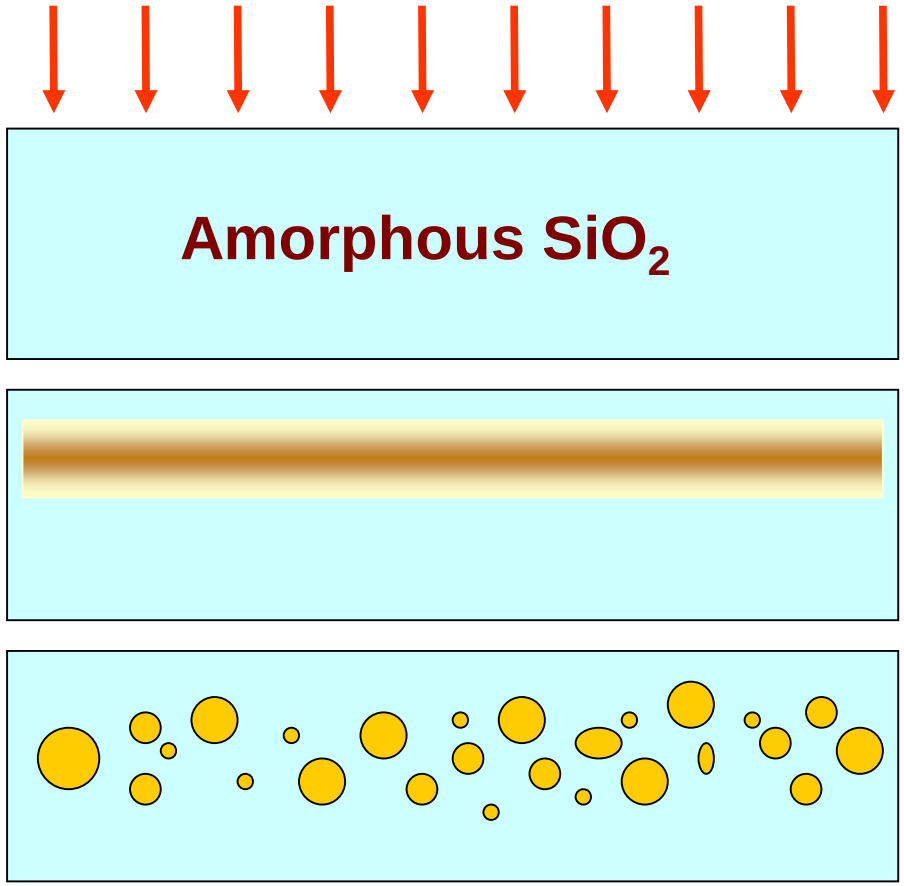

(a) Host material *implanted* with equal doses of group II and VI ions

(b) *Supersaturated solid solution* formed in the near surface region

(c) *nucleation of precipitates,* precipitates *grow* on the expense of incoming ion flux

d) during high-T annealing II-VI nanoparticles are being synthesized and in the process of Ostwald ripening agglomerating in discrete, isolated QD's of varying size

GISAXS pattern formation

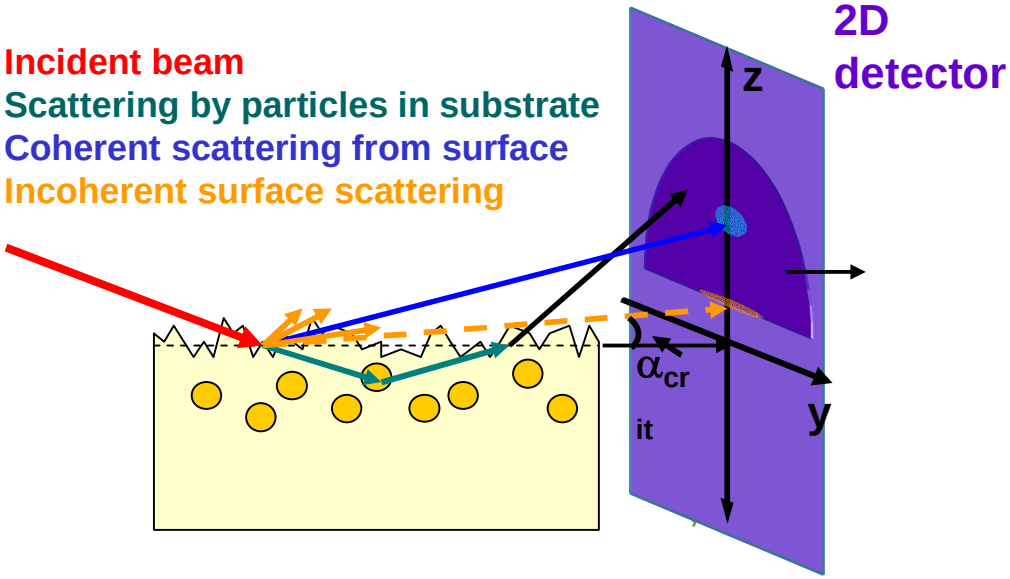

2D GISAXS pattern

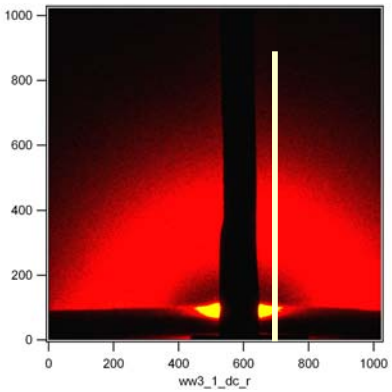

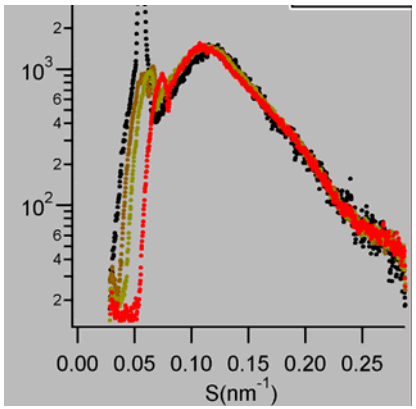

$\Lambda = 2\pi/q_m$, Λ = <u>average nanocrystals distance</u> - obtained from interference peak, $\boldsymbol{q}_{max}$

$\mathbf{R_g}$ = radius of gyration

$\Rightarrow$ D =<u>average cluster diameter</u>

obtained from slope of linear region of

I(q) versus q^2

Synthesis and growth of CdS Quantum Dots in SiO_2 studied by GISAXS

GISAXS-pattern

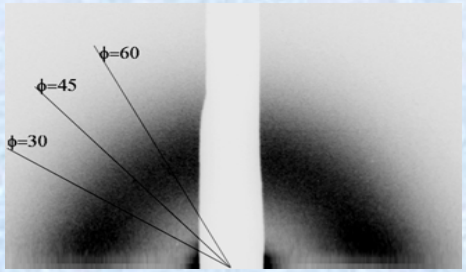

Intensity profiles

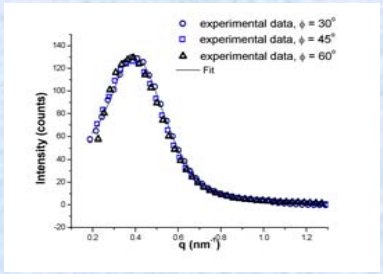

Isotropical distribution of spherical QDs with average diameter 8.8 nm, and with average distance of 10.8 nm

Concentration 5.3 exp 21/cm3

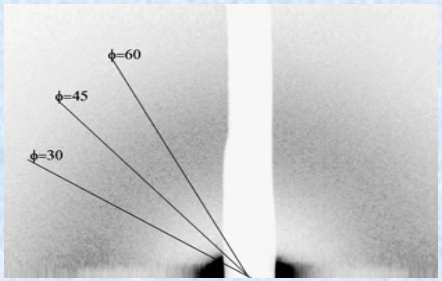

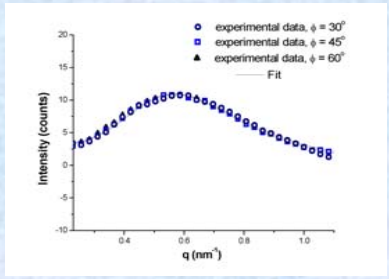

Isotropical distribution of spherical QDs with smaller average diameter and distance

Concentration 2.0 exp 21/cm3

LMA approximation, and DWBA formalism -> scattered intensity is:

$$I(q) \propto \left|T(\alpha_i)\right|^2 \left|T(\alpha_f)\right|^2 \int_0^\infty P(q,D) S(q, D_{hs}, \eta_{hs}) N(D,w) dD$$

U.V. Desnica, P. Dubcek, I.D. Desnica-Frankovic, M. Buljan, S. Bernstorff and C.W. White, J.Appl.Cryst. 36, 443-446 (2003)

Scattering from embedded particles:
Local Monodisperse Approximation - LMA

-system is approximated by monodisperse subsystems, weighted by the size distribution
-positions of the particles are completely correlated with their sizes

$$I(q) \propto |T(\alpha_i)|^2 |T(\alpha_f)|^2 \int_0^\infty P(q,D) S(q, D_{hs}, \eta_{hs}) N(D,w) dD$$

$T(\alpha_i)$ and $T(\alpha_f)$ - Fresnell transmission coefficients for angle of incidence α_i and exit α_f

P(q,D) - form factor of a homogeneous sphere of diameter D, (D=2R);

$S(q,D_{hs},\eta_{hs})$ - structure factor (η_{hs} - volume fraction and diameter of the hard spheres)

N(w,D) - Gaussian size distribution function

Surface scattering:
Distorted Wave Born Approximation - DWBA

$$I_{total} = I_{LMA} + I_{surface}$$

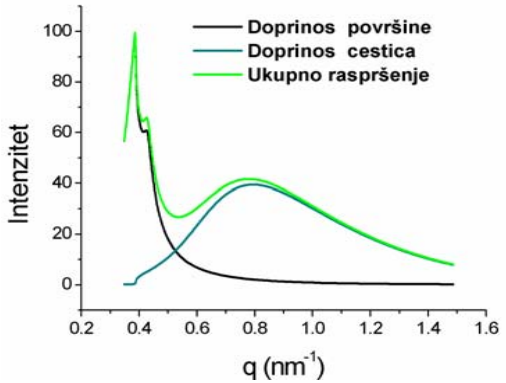

bimodal size distribution of particles – 1D GISAXS and TEM

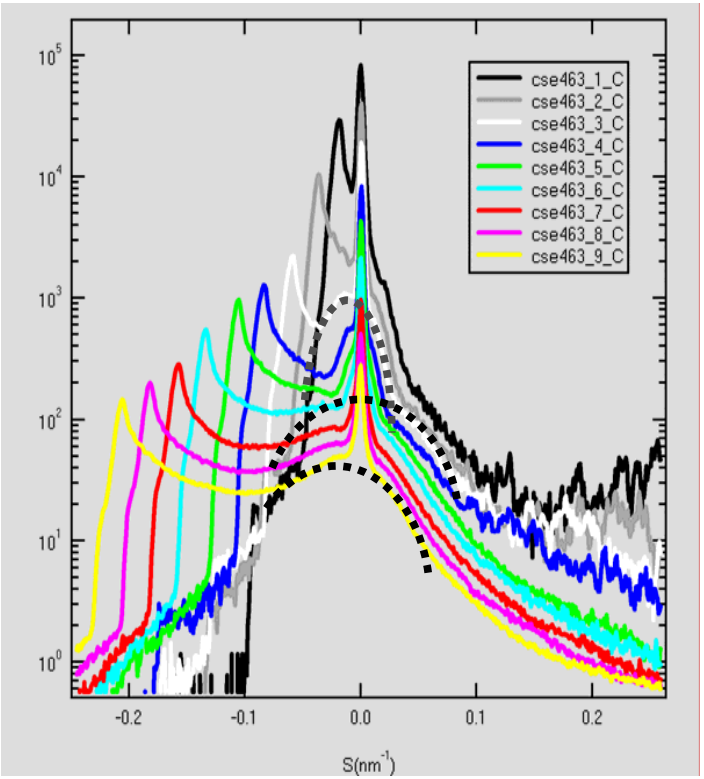

→ depth profiling by small increase of the incidence angle (0.02° step) ↓

closely spaced population of large particles with narrow size distribution $R_G \approx$ 50 -60 nmnm

shoulder - second group of smaller particles of broader size distribution $R_G \approx$ 5-7 nm

(**CdSe in SiO_2**, +0% Cd, 800 °C in Ar+H_2)

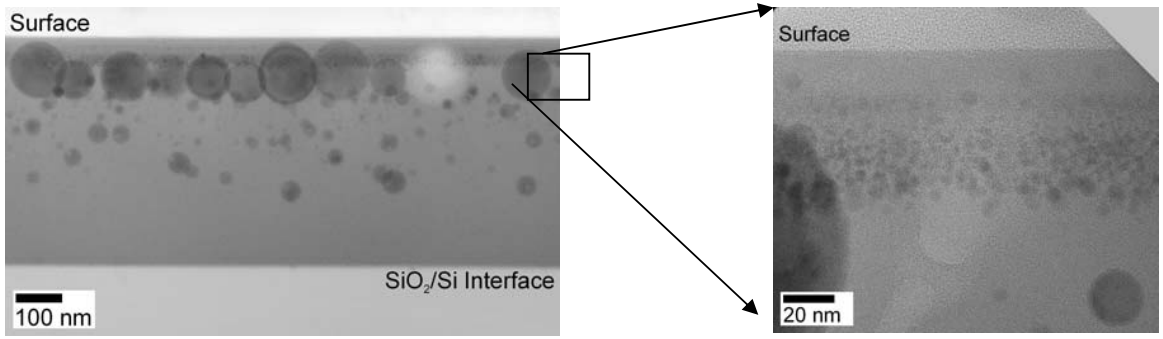

Cross-sectional **TEM** image:

Size distribution for **ZnSe nanocrystals in SiO_2** after annealing at 1000 °C, 30s, Ar**.** Sample was implanted with 33% surplus Cd. Among large particles positioned at approx. 100nm, there is also a band of small particles with diameters below 10 nm

2. Example: **GISAXS on thin $Ti0_2$ FILMS ON GLASS SUBSTRATE**

P. Dubcek, A. Turkovic, B. Etlinger, O. Milat, M. Lucic-Lavcevic, S. Bernstorff and H. Amenitsch

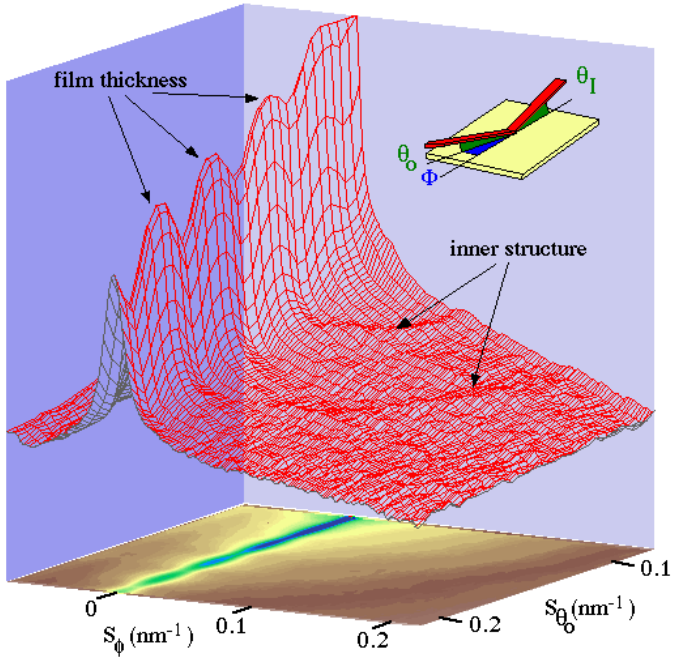

high correlation between the film and glass surface

➔ interference patterns in the specular plane (Φ=0)

➔ enables precise film thickness determination

concentric rings around the direct beam direction correspond to inner structure of the film

3. Example:

Grazing incidence X-ray scattering: an ideal tool to study quantum dot systems

GISAXS study of Ge islands on a Si(111) substrate

(T.H. Metzger et. Al, J. Phys. D: Appl. Phys. 32 (1999) A202-A207)

Sample prepared by molecular beam epitaxy at a substrate temperature of 530 °C.

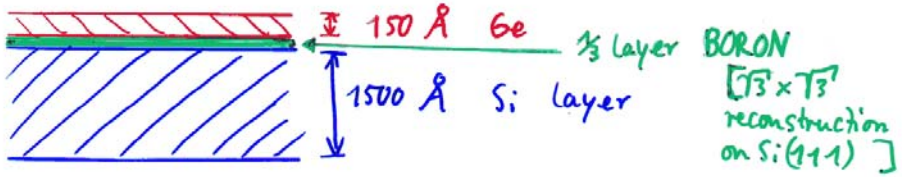

GISAXS

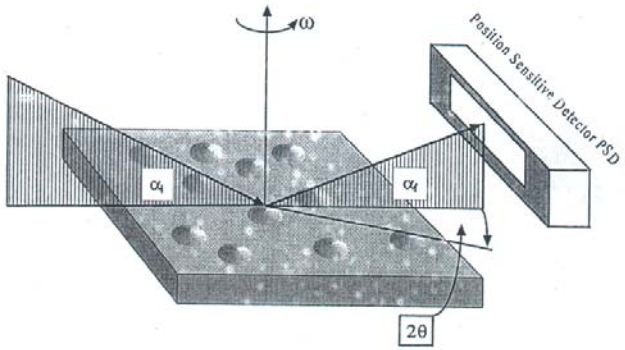

Figure 1. Scattering geometry for grazing incidence small angle scattering (GISAXS). The PSD is placed parallel to the sample surface : collects the small angle signal as a function of $q_{\parallel} = 2\pi/\lambda \sin(2\theta)$ at constant angles of incidence and exit, $\alpha_i \neq \alpha_f$. The axial symmetry the quantum dots are studied by rotating the azimuthal angle ω.

basic scattering geometry: $\alpha_i \approx \alpha_c$. The scattered signal is collected under grazing exit angles α_f in the forward direction with a 1D position sensitive detector (PSD) which is placed parallel to the sample surface.

The axial symmetry of the dots can be studied by varying the azimuthal angle ω keeping all other angles unchanged. Since $q_z \neq 0$ is typical for GISAXS, the full symmetry of the three-dimensional (3D) objects can be assessed in contrast to the conventional transmission SAXS with $q_z = 0$

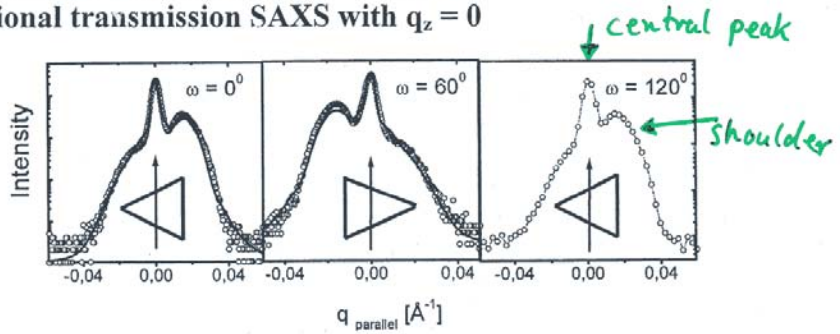

Figure 2. GISAXS signal from Ge pyramids on Si(111) for different azimuthal angles as a function of $q_{\parallel}$. The pyramids possess a threefold symmetry. The full curve is a fit to the experimental data (OOOO) using the structure factor of a pyramid (for details see [14]).

-> threefold symmetry properties of the scattering pattern -> threefold symmetry of triangular pyramids

From the relation between ω and the known <110> cleavage edge direction of the sample -> sides of pyramids are aligned along all possible <110> directions in the (111) oriented surface plane.

Fit of structure factor calculations to experimental data -> dimensions of the pyramids

AFM (atomic force microscopy) -> islands have pyramidal shape with well defined {113} facets; some exhibit also a small (111) terrace on the truncated top

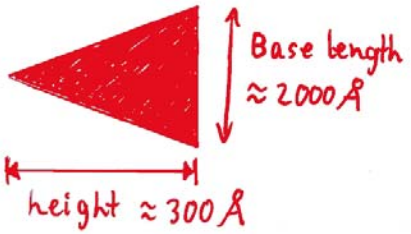

Grazing Incidence Diffraction (GID)

(T.H. Metzger et. Al, J. Phys. D: Appl. Phys. 32 (1999) A202-A207)

4. Example:

Example: InAs islands grown by molecular beam epitaxy on GaAs (100) at 530 °C substrate temperature

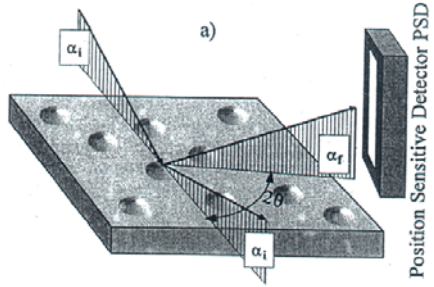

Scattering geometry for grazing incidence diffraction to study the crystalline properties of quantum dots. Three-dimensional reciprocal space maps are recorded in this geometry by collecting the scattered intensity as a function of the exit angle α_f, the scattering angle 2θ and the sample angle θ.

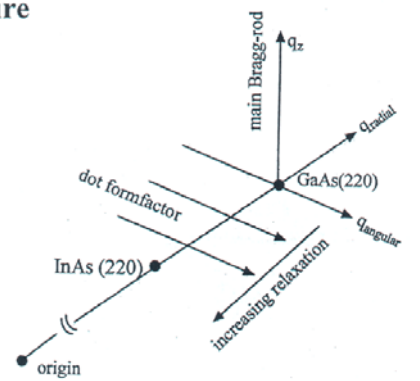

Important directions in reciprocal space close to the (220) surface Bragg reflections of GaAs and InAs. By adjusting q_r the lattice relaxation in the dots is measured, along q_a information on the lateral form factor of the dots is obtained, the q_z-dependence determines the maximum depth and reveals the form factor of the dots in the growth direction.

GID -> crystalline properties of coherent quantum dots

analysis of reciprocal space maps -> interdependence of shape and elastic strain within the quantum dots

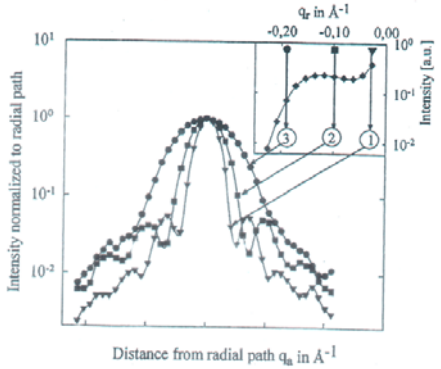

'Isostrain-scattering' between the (220) surface Bragg reflections of GaAs and InAs. The intensity distribution in angular scans is shown for different radial positions (q_r) as indicated in the inset. The angular dependence (q_a) of the scattering signal is characteristic for the lateral shape of the InAs dots. The central maximum broadens with increasing relaxation $|q_r|$

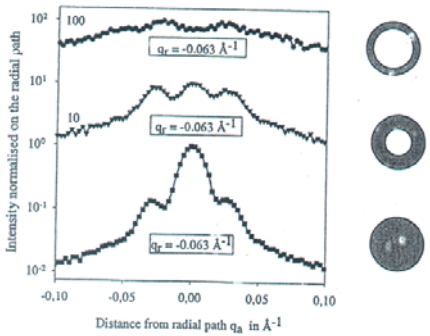

Form factor-induced scattering signal as a function of q_a for ring-shaped InAs islands overgrown by GaAs as a function of the relaxation q_r. The corresponding shapes of the islands are indicated schematically on the right-hand side.

Basic experimental considerations

Critical angles for e.g. 8 keV photons:

Organic films	$\alpha_c = 0.1^\circ \leftrightarrow 1.7$ mrad
Substrates	$\alpha_c = 0.2^\circ \leftrightarrow 3.4$ mrad

→ very flat substrates needed (e.g. silicon wafers, float glass)
→ very flat films (spin coating, dip coating, implanting, …) needed

Sample size (length L x width W)

Accepted beam height H
$H = L \cdot \alpha$
$L = 20$ mm, $\alpha = 0.2^\circ$
→ $H = 70\ \mu m$

W> beam width of ca 5 mm

Sample surrounding

- avoid scattered photons coming from slits etc …
- avoid scattered photons from air (i.e. work in vacuum, He-atmosphere, or use very short air paths):

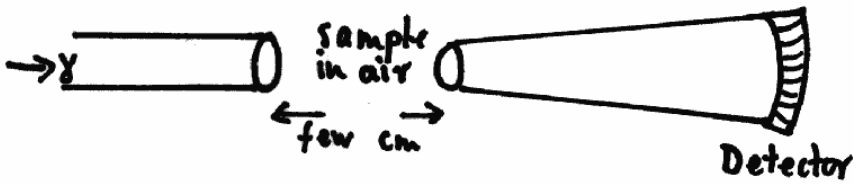

SUMMARY

There are several methods of X-ray scattering:

XRD	**->**	**- average strain** **- average composition** **- average chemical composition**
SAXS	**->**	**- shape, size, distribution and distances of structures in amorphous or partly ordered sample systems (bulk informations)**
XRR	**->**	**- surface and interfaces** **- roughness** **- correlations** **- layer thicknesses**
GISAXS	**->**	**- shape, size, distribution and distances (lateral correlations) of nanostructures on surfaces, interfaces and thin films**
GID	**->**	**- crystalline properties of coherent quantum dots** **- in-plane strain** **- depth dependent strain** **- composition**

Small-angle x-ray scattering under grazing incidence: The cross section in the distorted-wave Born approximation

M. Rauscher, T. Salditt, and H. Spohn
Sektion Physik der Ludwig-Maximilians-Universität München, Geschwister-Scholl-Platz 1, 80539 München, Germany
(Received 11 April 1995; revised manuscript received 28 August 1995)

The specular and nonspecular intensity of x rays scattered from a rough surface with fluctuations in the electron density is calculated in the distorted-wave Born approximation. The contributions to the nonspecular intensity of roughness and density fluctuations can be separated. The structure factor is given by a convolution integral of the Fourier transform of the density correlation function. Special geometries of density fluctuations are discussed.

I. INTRODUCTION

Small-angle x-ray scattering (SAXS) is a fully developed and well established method to investigate density fluctuations on length scales from 10 Å to several thousand Å.[1] In contrast to real-space microscopy, SAXS determines statistically averaged quantities, such as density correlations. Experiments are usually performed in transmission geometry; i.e., the sample is put in the primary beam and the scattering intensity is measured behind the sample close to the forward direction in the vicinity of the direct beam.

For many applications, conventional SAXS suffers from two major drawbacks: First, an oftentimes poor resolution at the low end of momentum transfer and second, a lack of surface sensitivity.

As far as the first point is concerned, the resolution at low momentum transfer is limited by the finite size of the primary beam. Even if the half with of the beam is very small, as is the case for most modern synchrotron sources, the intensity tails of the beam as observed on a logarithmic scale contaminate the scattering signal at small angles. In practice, this effect limits the spatial length scale that can be probed to be less than about 1000–2000 Å for most instruments and samples. On the contrary, it has been shown that under grazing incidence even by hard x rays of wavelength $\lambda \approx 1$ Å, much longer length scales of up to 10–100 μm are accessible, if a suitable scattering geometry is chosen.[2,3] This has been demonstrated by the observation of diffraction maxima from synthetic surface gratings with μm periodicities, and can be explained by the different relationship between the scattering angle and momentum transfer in both scattering geometries. Thus, for structural characterization on long length scales, it is promising to measure the so-called *nonspecular* or *diffuse* scattering, i.e., the small-angle scattering in the vicinity of the specularly reflected beam. Of course, in the μm range, light scattering can be employed to deduce structural information. However, this technique does not work for opaque materials.

The second drawback is simply due to the fact that in transmission geometry the beam has to pass through the whole bulk of the sample. Thus, the contributions of surface roughness and other near-surface structures are negligible in all but a very few cases as compared to the bulk signal. However, in recent years the interest in surface and near-surface phenomena has created an increasing demand for surface-sensitive characterization. One may have a number of examples in mind where spatial fluctuations of the electron density occur only near or at the surface, or where such fluctuations are to be studied under the influence of the surface, e.g., precipitation of ion-implanted dopant atoms in single crystals, thin layers of porous silicon, segregation in a binary alloy, polymer adsorption on a surface, Langmuir films, etc. It is therefore of interest to combine small-angle scattering with the well-known surface sensitivity of grazing incidence diffraction.[4] The first experiment of this kind has been reported in 1989 by Levine *et al.*, who have studied the growth of gold islands on glass. Nonspecular scattering of Langmuir-Blodgett films has also been attributed to lateral fluctuations.[5]

However, the quantitative analysis of experimental data requires as suitable theory of the scattering process, which is available only for relatively simple objects like periodic surface gratings or some other special configurations. The classical formulas of small-angle scattering[6] cannot be expected to hold, as refraction effects and in particular an eventually complex momentum transfer have to be taken into account. The theoretical basis can be improved by starting from a general expression for the scattered wave in the framework of the distorted-wave Born approximation (DWBA). The main goal of our paper is to illustrate the general result for particular geometries of physical interest. In particular, we want to understand how the various types of density fluctuations can be unambiguously distinguished by means of their scattering intensity distribution.

One of the most prominent density fluctuations is surface roughness. Indeed, nonspecular scattering of rough surfaces was the first kind of small-angle scattering to be described theoretically. In 1988, Sinha and co-workers calculated the scattering cross section of a rough surface in DWBA, thereby starting a rapidly increasing activity in the filed of roughness characterization.[7] Whereas be-

fore only the electron density along the surface normal had been studied, with this theory at hand also lateral quantities of roughness could be determined. The experimental method is often referred to simply as *diffuse scattering*.

A master formula including both surface roughness and density fluctuations has been derived by Dietrich and Haase[8] (earlier efforts for particular cases are described in Refs. 9–11). However, their very general result has not been applied to the geometries considered in this paper. In order to keep the notation close to Ref. 7 and for the sake of conceptual clarity, we present here a self-contained discussion of the scattering process. We point out that our results can be generalized for the case of neutron scattering in a straightforward manner.

The paper is organized as follows: In Sec. II we use the distorted-wave Born approximation to calculate the scattered wave from a rough surface with additional bulk density fluctuations and we discuss conditions under which correlations between these two contributions can be neglected. In Sec. III we apply the general result to lateral density variations at planar surface, to columnar disorder, and isotropically distributed spherical inclusions in the bulk as well as to a buried layer of density fluctuations. Finally, some concluding remarks are found in Sec. IV.

II. DISTORTED-WAVE BORN APPROXIMATION

A. The scattering amplitude

Let us consider a semi-infinite medium extending over the lower half space $z<0$ with the average surface lying in the xy plane. The deviation of the surface from its mean is parametrized by the function $h(\mathbf{r}_\parallel)$ with $\mathbf{r}_\parallel=(x,y)$. The medium is characterized by an average index of refraction n and is assumed to be homogeneous except for the presence of surface roughness and density fluctuations. The amplitude $w(\mathbf{r})$ of the density fluctuations describes the local deviation from the average index of refraction.

Let us now assume an x-ray beam impinging on the surface with an extension much larger than the coherence length. Then the amplitudes scattered from parts of the sample separated by distances larger than the coherence length add up incoherently and the scattering intensity is determined by a spatial average. Assuming erogodicity it can be substituted by a configurational average denoted as $\langle\cdot\rangle$. The statistics of h and w are assumed to be isotropic and translational invariant in the xy direction. Thus, we have $\langle h(x,y)\rangle=0$ and $\langle w(\mathbf{r})\rangle=\langle w\rangle(z)$. Moreover, we choose $\langle\omega\rangle(z)=0$ for $z\to-\infty$, since any offset $\bar{w}$ from w can be used to renormalize the average index of refraction.

The incident wave is described by a wave vector $\mathbf{k}_i$ with modulus k_0 (corresponding to the vacuum wavelength $\lambda=2\pi/k_0$) and the scattered wave by $\mathbf{k}_f$ of equal modulus (Fig. 1). The scattering vector is denoted by $\mathbf{q}=\mathbf{k}_f-\mathbf{k}_i$. To distinguish the wave vectors in the medium they carry a tilde, i.e., $\tilde{\mathbf{k}}_i$, $\tilde{\mathbf{k}}_f$, and $\tilde{\mathbf{q}}$. Due to refraction and absorption they may be complex. For small

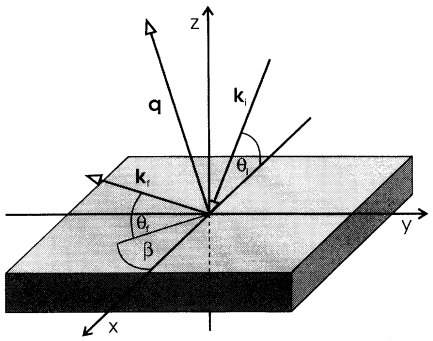

FIG. 1. Scattering of x rays under grazing incidence. The incident wave vector $\mathbf{k}_i$, the reflected wave vector $\mathbf{k}_f$, and the scattering vector $\mathbf{q}$ are illustrated. θ_i and θ_f are the angles of incidence and exit, respectively; β is the angle between the plane of incidence and the projection of the final wave vector on the surface.

scattering angles with $2\pi/q$ greater than typical interatomic distances, the atomic structure of the medium can be neglected. Furthermore, for such small scattering angles and for an index of refraction $n\approx1$ polarization effects can be ignored, i.e., electromagnetic waves behave like scalar waves. This is a valid approximation for hard x rays, since $1-n$ is of the order 10^{-6}.

The amplitude of the electromagnetic field satisfies the stationary wave equation

$$(\Delta+k_0^2-V-W)\Psi=0\ , \tag{1}$$

with $V(z)=k_c^2\Theta(-z)$ and $k_c^2=k_0^2(1-n^2)$. Here $\Theta(-z)$ denotes the Heaviside function and k_c is the vertical component of the momentum vector at the critical angle θ_c of total external reflection. The ideal surface, equal to the xy plane, is described by the potential V, surface roughness, and density fluctuations by W. The perturbation W has the following form:

$$W(\mathbf{r})=k_c^2\{\Theta[h(\mathbf{r}_\parallel)-z]\Theta(z)-\Theta[z-h(\mathbf{r}_\parallel)]\Theta(-z) +w(\mathbf{r})\Theta[h(\mathbf{r}_\parallel)-z]\}\ . \tag{2}$$

The first two terms on the right-hand side correspond to surface roughness, the third term to density fluctuations, as illustrated in Fig. 2.

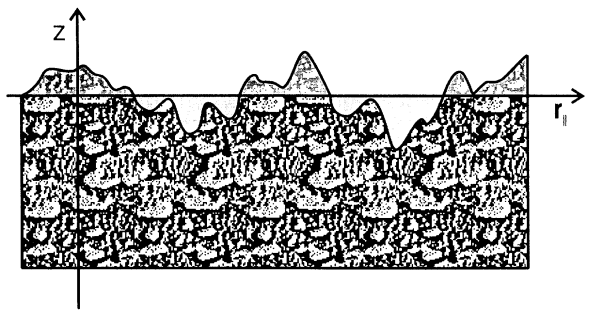

FIG. 2. Schematic of a rough surface with density fluctuations. The average surface lies in the xy plane. Surface roughness and density fluctuations are the two kinds of disorder considered.

Without W, Eq. (1) describes the scattering of scalar waves from a planar surface and is solved by the Fresnel function

$$\Psi^{(0)}(\mathbf{r},\mathbf{k})=e^{i\mathbf{k}_\parallel\cdot\mathbf{r}_\parallel}\begin{cases} e^{ik_\perp z}+\mathcal{R}e^{-ik_\perp z}, & \text{if } z>0 \\ \mathcal{T}e^{i\tilde{k}_\perp z}, & \text{if } z<0 \end{cases} \tag{3}$$

for an incoming plane wave with $\mathbf{k}=(\mathbf{k}_\parallel,k_\perp)$ and $k_\perp=-\sqrt{k_0^2-|\mathbf{k}_\parallel|^2}$. The vertical component of the bulk wave vector is $\tilde{k}_\perp=-\sqrt{k_0^2-k_c^2-|\mathbf{k}_\parallel|^2}$ and the Fresnel reflectivity $\mathcal{R}$ and transmittivity $\mathcal{T}$ are given by

$$\mathcal{T}=\frac{2k_\perp}{k_\perp+\tilde{k}_\perp} \text{ and } \mathcal{R}=\frac{k_\perp-\tilde{k}_\perp}{k_\perp+\tilde{k}_\perp} . \tag{4}$$

Using the Green's function,

$$(\Delta+k_0^2-V)G^{(+)}(\mathbf{r},\mathbf{r}',k_0^2)=\delta(\mathbf{r}-\mathbf{r}') \tag{5}$$

for outgoing waves, we transform Eq. (1) to the Lippmann-Schwinger equation

$$\Psi(\mathbf{r})=\Psi^{(0)}(\mathbf{r})+\int d^3r'G^{(+)}(\mathbf{r},\mathbf{r}',k_0^2)W(\mathbf{r}')\Psi(\mathbf{r}') . \tag{6}$$

In the far field the Green's function is given by Refs. 8, 14, 18, and 19 and Ref. 20, Appendix B,

$$G^{(+)}(\mathbf{r},\mathbf{r}',k_0)\sim-\frac{e^{ik_0r}}{4\pi r}\Psi^{(0)}(\mathbf{r}',-\mathbf{k}_f) \text{ for } z\to\infty . \tag{7}$$

We assume that Ψ in Eq. (6) can be expanded in powers of W and solve Eq. (6) by a recursion procedure starting with $\Psi^{(0)}(\mathbf{r},\mathbf{k}_i)$ which is the solution of the unperturbed system for an incoming wave with wave vector $\mathbf{k}_i$. Up to first order we get in the far field

$$\Psi(\mathbf{r})=\Psi^{(0)}(\mathbf{r},\mathbf{k}_i)-\frac{e^{ik_0r}}{4\pi r}\int d^3r'\Psi^{(0)}(\mathbf{r}',-\mathbf{k}_f)\times W(\mathbf{r}')\Psi^{(0)}(\mathbf{r}',\mathbf{k}_i) . \tag{8}$$

Since the DWBA is valid only for small roughness $\sigma=\sqrt{\langle h^2\rangle}$ (Ref. 7) and since the solution $\Psi^{(0)}$ of the unperturbed system [Eq. (1) with $W=0$] is continuous at $z=0$, we make the following approximation:[7,12,13] The field above the xy plane but inside the sample is given by the transmitted part of the Fresnel solutions. Since the integration in Eq. (8) does not exceed the z range where the approximation is valid, we may substitute $\Psi^{(0)}(\mathbf{r}',-\mathbf{k}_f)$ and $\Psi^{(0)}(\mathbf{r}',\mathbf{k}_i)$ by $\mathcal{T}_fe^{-i\tilde{\mathbf{k}}_f\cdot\mathbf{r}}$ and $\mathcal{T}_ie^{i\tilde{\mathbf{k}}_i\cdot\mathbf{r}}$, respectively, where $\mathcal{T}_i$ and $\mathcal{T}_f$ are the Fresnel transmission coefficients for plane waves with a wave vector $\mathbf{k}_i$ and $-\mathbf{k}_f$ as given in Eq. (4). Thus, the scattered wave can be written as

$$\Psi(\mathbf{r})=\Psi^{(0)}(\mathbf{r},\mathbf{k}_i)-\frac{e^{ik_0r}}{4\pi r}\mathcal{T}_i\mathcal{T}_f\int d^2r'_\parallel e^{-i\mathbf{q}_\parallel\cdot\mathbf{r}'_\parallel}\times\int_{-\infty}^{+\infty}dz'e^{-i\bar{q}_\perp z'}W(\mathbf{r}') . \tag{9}$$

Substituting W from Eq. (2) we get

$$\Psi(\mathbf{r})=\Psi^{(0)}(\mathbf{r},\mathbf{k}_i)-\frac{e^{ik_0r}}{4\pi r}k_c^2\mathcal{T}_i\mathcal{T}_f\int d^2r'_\parallel e^{-i\mathbf{q}_\parallel\cdot\mathbf{r}'_\parallel}\left[\int_0^{h(\mathbf{r}'_\parallel)}dz'e^{-i\bar{q}_\perp z'}+\int_{-\infty}^{h(\mathbf{r}'_\parallel)}dz'e^{-i\bar{q}_\perp z'}w(\mathbf{r}'_\parallel,z')\right] . \tag{10}$$

For small surface roughness σ we replace the second integral by

$$\int_{-\infty}^{0}dz'e^{-i\bar{q}_\perp z'}w(\mathbf{r}'_\parallel,z') . \tag{11}$$

This approximation would be invalid if the density fluctuations were located exclusively in a range of $\pm\sigma$ relative to the xy plane. Within this approximation the scattered amplitude has two independent parts, one from the surface roughness and one from the density fluctuations

$$\Psi-\Psi^{(0)}(\mathbf{k}_i)\approx\Psi_s+\Psi_d , \tag{12}$$

where

$$\Psi_s=-\frac{e^{ik_0r}}{4\pi r}k_c^2\mathcal{T}_i\mathcal{T}_f\int d^2r'_\parallel e^{-i\mathbf{q}_\parallel\cdot\mathbf{r}'_\parallel}\int_0^{h(\mathbf{r}'_\parallel)}dz'e^{-i\bar{q}_\perp z'} , \tag{13}$$

$$\Psi_d=-\frac{e^{ik_0r}}{4\pi r}k_c^2\mathcal{T}_i\mathcal{T}_f\int d^2r'_\parallel e^{-i\mathbf{q}_\parallel\cdot\mathbf{r}'_\parallel}\times\int_{-\infty}^{0}dz'e^{-i\bar{q}_\perp z'}w(\mathbf{r}'_\parallel,z') . \tag{14}$$

To calculate the scattered intensity we have to perform the configurational average as explained above. The averaged intensity $\langle|\Psi|^2\rangle=\langle\Psi^{(0)}(\mathbf{k}_i)+\Psi_s+\Psi_d\rangle$ can be written as follows:

$$\langle|\Psi|^2\rangle=|\Psi^{(0)}+\langle\Psi_s\rangle+\langle\Psi_d\rangle|^2+\langle|\Psi_s|^2\rangle-|\langle\Psi_s\rangle|^2+\langle|\Psi_d|^2\rangle-|\langle\Psi_d\rangle|^2+2\,\mathrm{Re}(\langle\Psi_s\Psi_d^*\rangle-\langle\Psi_s\rangle\langle\Psi_d^*\rangle) . \tag{15}$$

The first term describes the specularly reflected intensity. The other terms are the diffuse intensities written as a sum of contributions from the surface roughness, from the density fluctuations, and from their intercorrelations.

B. scattering intensity and structure factor

1. Specular intensity

The specularly reflected intensity depends only on averaged amplitudes. Obviously the contributions from the density fluctuations are proportional to $\langle w\rangle$. Thus this term gives the specular reflected intensity since we only allow density fluctuations with $\langle w(\mathbf{r})\rangle=\langle w\rangle(z)$. For the contributions from the surface roughness the

complete statistics of h is needed and explicit formulas are available for surfaces with Gaussian statistics.[7,14]

Due to our choice $\langle w \rangle(z)=0$ for $z\to-\infty$ for homogeneous density fluctuations $\langle w(\mathbf{r})\rangle=0$ and give no contribution to the specularly reflected intensity. Besides such homogeneous density fluctuations we will discuss the case where the density fluctuations are restricted to a certain layer between $z=a$ and $z=b$. Thus we substitute w by

$$\Theta(z-a)\Theta(b-z)w(\mathbf{r}_\parallel,z)\ , \tag{16}$$

$0\geq b>a$, with $\langle w(\mathbf{r}_\parallel,z)\rangle=\text{const}=\bar{w}$. This corresponds to a modulation of the index of refraction in z.

The specular part of the scattered intensity is then given by

$$\begin{aligned}|\Psi^{(0)}+\langle\Psi_s\rangle+\langle\Psi_d\rangle|^2 &= \left|\Psi^{(0)}+\langle\Psi_s\rangle-\frac{e^{ik_0 r}}{4\pi r}k_c^2\bar{w}\mathcal{T}_i\mathcal{T}_f\right. \\ &\left.\times(2\pi)^2\delta(\mathbf{q}_\parallel)\frac{i}{\bar{q}_\perp}(e^{-i\bar{q}_\perp b}-e^{-i\bar{q}_\perp a})\right|^2 .\end{aligned} \tag{17}$$

In the far field for $z\to\infty$, the rightmost term has the asymptotic form of a plane wave with wave vector $\mathbf{k}_f=(\mathbf{k}_{\parallel i},-\mathbf{k}_{\perp i})$ and amplitude[15]

$$k_c^2\bar{w}\mathcal{T}_i\mathcal{T}_f\frac{1}{q_\perp\bar{q}_\perp}(e^{-i\bar{q}_\perp b}-e^{-i\bar{q}_\perp a})e^{i\mathbf{k}_f\cdot\mathbf{r}}\ . \tag{18}$$

According to Ref. 7 the first two terms in the specular intensity can be combined to a wave field similar to the Fresnel solutions with a modified reflection coefficient $\mathcal{R}e^{-1/2q_\perp\bar{q}_\perp\sigma^2}$ which is obtained in Ref. 16 by a different method. This reflection coefficient is defined as the amplitude of the outgoing wave divided by the amplitude of the incoming wave. Thus the complete reflection coefficient for our geometry is given by

$$\mathcal{R}e^{-1/2q_\perp\bar{q}_\perp\sigma^2}+k_c^2\bar{w}\mathcal{T}_i\mathcal{T}_f\frac{1}{q_\perp\bar{q}_\perp}(e^{-i\bar{q}_\perp b}-e^{-i\bar{q}_\perp a})\ . \tag{19}$$

The reflectivity measured in an experiment is the square of the modulus of the reflection coefficient above.

2. Nonspecular intensity

The nonspecular scattering intensity will be calculated for the case of statistically independent w and h. Strong correlations between w and h would make the interpretation of measured intensities rather difficult. Anyhow, in many experimental situations, one of the two contributions is small as compared to the other. The cross term in (15) is given by

$$\frac{k_c^4}{(4\pi r)^2}|\mathcal{T}_i|^2|\mathcal{T}_f|^2 2\,\mathrm{Re}\left[\frac{i}{\bar{q}_\perp}\int d^2r'_\parallel\int d^2r''_\parallel\int_{-\infty}^0 dz''e^{i\bar{q}_\perp^*z''}(\langle e^{-i\bar{q}_\perp h(\mathbf{r}'_\parallel)}w(\mathbf{r}'')\rangle-\langle e^{-i\bar{q}_\perp h(\mathbf{r}'_\parallel)}\rangle\langle w(\mathbf{r}'')\rangle)\right] \tag{20}$$

and vanishes by assumption. The diffuse intensity in (15) reduces then to $\langle|\Psi_s|^2\rangle-|\langle\Psi_s\rangle|^2+\langle|\Psi_d|^2\rangle-|\langle\Psi_d\rangle|^2$, the sum of the intensities scattered by surface roughness and density fluctuations.

For rough surfaces with Gaussian statistics, the surface contributions can be evaluated analytically. With the height correlation function $C_h(|\mathbf{r}'_\parallel-\mathbf{r}''_\parallel|)=\langle h(\mathbf{r}'_\parallel)h(\mathbf{r}''_\parallel)\rangle$ we have[7,14]

$$\langle|\Psi_s|^2\rangle-|\langle\Psi_s\rangle|^2=\frac{k_c^4}{(4\pi r)^2}|\mathcal{T}_i|^2|\mathcal{T}_f|^2L_xL_y\frac{1}{|\bar{q}_\perp|^2}e^{-\sigma^2/2(\bar{q}_\perp^2+\bar{q}_\perp^{*2})}\int d^2R_\parallel e^{-i\mathbf{q}_\parallel\cdot\mathbf{R}_\parallel}(e^{|\bar{q}_\perp|^2C_h(\mathbf{R}_\parallel)}-1)\ , \tag{21}$$

where $\mathbf{R}_\parallel=\mathbf{r}'_\parallel-\mathbf{r}''_\parallel$. Here L_x and L_y are the lengths of the illuminated area of the sample in the x and y directions. Both L_x and L_y are assumed to be large as compared to the vacuum wavelength $2\pi/k_0$.

Using the density correlation function which is defined as $C_w(|\mathbf{r}'_\parallel-\mathbf{r}''_\parallel|,z',z'')=\langle w(\mathbf{r}'_\parallel,z')w(\mathbf{r}''_\parallel,z'')\rangle$, the diffuse intensity from the bulk is for $\mathbf{q}_\parallel\neq0$

$$\langle|\Psi_d|^2\rangle-|\langle\Psi_d\rangle|^2=\frac{k_c^4}{(4\pi r)^2}|\mathcal{T}_i|^2|\mathcal{T}_f|^2L_xL_y\int d^2R_\parallel e^{-i\mathbf{q}_\parallel\cdot\mathbf{R}_\parallel}\int_{-\infty}^0 dz'\int_{-\infty}^0 dz''e^{-i\bar{q}_\perp z'+i\bar{q}_\perp^*z''}C_w(|\mathbf{R}_\parallel|,z',z'')\ . \tag{22}$$

The scattered intensity is proportional to an integral transform similar to the Fourier transform of the density correlation function C_w. By homogeneity, C_w depends only on $|\mathbf{r}'_\parallel-\mathbf{r}''_\parallel|$. In the transverse direction we have a general dependence on both z' and z'', unless $\langle w\rangle=\text{const}$, e.g., away from the surface.

The intensity is proportional to the squared moduli of the Fresnel transmission coefficients. This leads to the so-called Yoneda peaks whenever the angle of incidence or exit equals the critical angle. The same effect can be observed in the scattering from rough surfaces [see Eq. (21)].[17]

At this point we introduce the differential cross section $d\sigma/d\Omega$ and the diffuse structure factor $S(\mathbf{q})$, which are defined as follows [Ref. 8, Eq. (4.26)]:

$$\begin{aligned}\langle|\Psi_d|^2\rangle-|\langle\Psi_d\rangle|^2&=\frac{1}{r^2}\frac{d\sigma}{d\Omega}\\&=\frac{k_c^4}{(4\pi r)^2}|\mathcal{T}_i|^2|\mathcal{T}_f|^2L_xL_yS(\mathbf{q})\ .\end{aligned} \tag{23}$$

Thus for the diffuse structure factor S we have

$$S(\mathbf{q})=\int d^2R_{\parallel}e^{-i\mathbf{q}_{\parallel}\cdot\mathbf{R}_{\parallel}}\int_{-\infty}^{0}dz'\int_{-\infty}^{0}dz''e^{-i\tilde{q}_{\perp}z'+i\tilde{q}_{\perp}^{*}z''}\times C_w(|\mathbf{R}_{\parallel}|,z',z'')\ , \tag{24}$$

for $\mathbf{q}_{\parallel}\neq 0$. In the following section we will calculate the structure factors for four representative examples of correlation functions.

III. GEOMETRIES OF DENSITY FLUCTUATIONS

In Sec. II B we derived a master formula [Eq. (24)] for the diffuse structure factor. In order to illustrate this result we discuss four different configurations of density fluctuations which are characterized by specific restrictions on the symmetry of the correlation function C_w. These four models are displayed in Fig. 3. We first discuss the case of perturbations located in a δ-like layer at the top of the surface [Fig. 3(a)], e.g., variations in the density of adsorbed atoms. Second, we expand the lateral pattern to the whole bulk, such that the density fluctuations are constant in the z direction [Fig. 3(b)]. This geometry would be appropriate to describe columnar structures. In the third more general case, we assume isotropic density fluctuations with a translational symmetry in all three directions [Fig. 3(c)]. We will show that in the limit $\mathrm{Im}\tilde{q}_{\perp}\rightarrow\infty$, the structure factor of this model reduces to the previous one. In the last configuration, we restrict the density fluctuations of the third model to a layer of finite thickness parallel to the average surface [Fig. 3(d)]. In fact, this is the most general model from which all previous structure factors can be derived. But for the sake of clarity we discuss the simpler configurations first.

A. δ layer

Assuming density fluctuations $w(\mathbf{r}_{\parallel})\delta(z)t$ located at the surface of the sample [Fig. 3(a)] the correlation function becomes

$$C_w(\mathbf{R}_{\parallel})\delta(z')\delta(z'')t^2\ , \tag{25}$$

where t denotes the thickness of the so-called δ layer. In this case the contribution of the density fluctuations and of surface roughness, respectively, cannot be treated independently as in Eq. (10). Therefore, we assume a perfectly flat surface $h(\mathbf{r}_{\parallel})=0$ and obtain

$$S(\mathbf{q})=\int d^2R_{\parallel}e^{-i\mathbf{q}_{\parallel}\cdot\mathbf{R}_{\parallel}}C_w(\mathbf{R}_{\parallel})t^2=\hat{C}_w(\mathbf{q}_{\parallel})t^2\ . \tag{26}$$

Here a "hat" indicates a Fourier transform. This formula has been derived before to describe the scattering of soft x rays from almost smooth surfaces.[9,10] In the limit of $\sigma^2|\tilde{q}_{\perp}|^2\rightarrow 0$ a rough surface cannot be distinguished from a surface with such density fluctuations.

To illustrate Eq. (26) let us calculate the structure factor as corresponding to the correlation function of a disk with radius R,

$$\hat{C}_w(\mathbf{q}_{\parallel})=\left[\frac{2\pi R}{|\mathbf{q}_{\parallel}|}J_1(|\mathbf{q}_{\parallel}|R)\right]^2\ . \tag{27}$$

Here J_1 denotes the first Bessel function of the first kind. For the example presented in Fig. 4 the radius of the disk is assumed to be $R=1000\lambda$ and the index of refraction $n=1-6.1\times10^{-6}+i\times10^{-7}$, corresponding to a critical angle of total external reflection of $\theta_c=0.2°$. The structure factor is plotted at constant angle of incidence $\theta_i=0.5°$ as a function of the exit angle θ_f and the angle β (out of the plane of incidence). Except for the effect of the transmission functions, Fig. 4 shows the intensity as measured on a two-dimensional detector behind the sample. The oscillations along β correspond to the radius of the disks.

B. Columnar model

For $\omega(\mathbf{r}_{\parallel},z')=w(\mathbf{r}_{\parallel})$, i.e., density fluctuations constant along the transverse direction, the structure factor is given by

$$S(\mathbf{q})=\frac{1}{|\tilde{q}_{\perp}|^2}\hat{C}_w(\mathbf{q}_{\parallel})\ . \tag{28}$$

The only difference to the structure factor of the δ layer is the decay in $|\tilde{q}_{\perp}|$.

For the plot in Fig. 5 we chose the same correlation

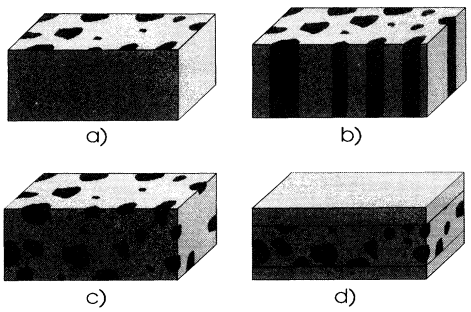

FIG. 3. Illustration of the four discussed restrictions on the geometry of the density fluctuations. A δ-like layer at the surface (a), columnar structures (b), isotropic density fluctuations (c), and a layered structure (d).

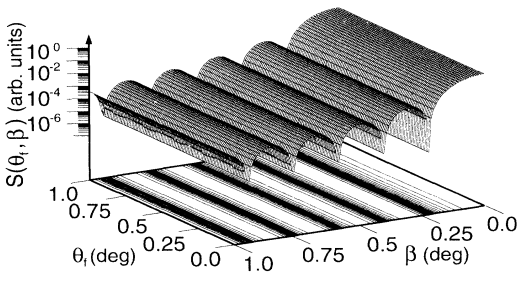

FIG. 4. The diffuse structure factor for a δ-like layer of spherical disks with radius $R=1000\lambda$ is plotted as a function of β and θ_f. The angle of incidence is chosen, $\theta_i=0.5°$, and the medium is assumed to have an index of refraction of $n=1-6.1\times10^{-6}+i\times10^{-7}$.

function and the same parameters as for the δ layer. In the calculated structure factor a change of slope is observed at the critical angle $\theta_f=\theta_c$ which should not be mixed up with the Yoneda wings.

C. Isotropic density fluctuations

To discuss a more general case we assume a correlation function of the form $C_w=C_w(|\mathbf{R}_\parallel|,|Z|)$ with $Z=z'-z''$, i.e., density fluctuations which are both laterally and vertically homogeneous. Thus surface effects that extend over a length smaller than the bulk correlation length ξ can be neglected here. The structure factor is no longer a simple Fourier transform of the correlation function as in the previous subsections. Splitting the (z',z'') integration in Eq. (24) into two parts and interchanging the names of z' and z'' in the second integral, we have

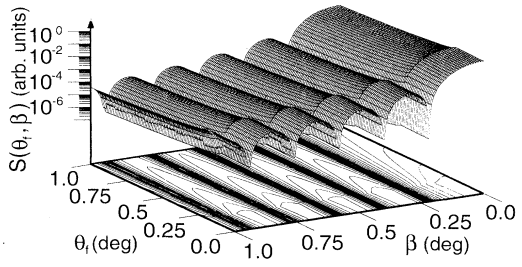

FIG. 5. The diffuse structure factor for columnar structures with the same correlation function as in Fig. 4 plotted as a function of β and θ_f. The radius is $R=1000\lambda$, the angle of incidence $\theta_i=0.5°$, and the index of refraction $n=1-6.1\times10^{-6}+i\times10^{-7}$.

$$S(\mathbf{q})=\int d^2R_\parallel e^{-i\mathbf{q}_\parallel\cdot\mathbf{R}_\parallel}\left[\int_0^\infty dz''\int_{z''}^\infty dz' e^{-i\,\mathrm{Re}\tilde{q}_\perp(z'-z'')}e^{-\mathrm{Im}\tilde{q}_\perp(z'+z'')}C_w(|\mathbf{R}_\parallel|,|z'-z''|)\right.$$
$$\left.+\int_0^\infty dz''\int_{z''}^\infty dz' e^{i\,\mathrm{Re}\tilde{q}_\perp(z'-z'')}e^{-\mathrm{Im}\tilde{q}_\perp(z'+z'')}C_w(|\mathbf{R}_\parallel|,|z'-z''|)\right]. \tag{29}$$

After substitution of z' by $Z=|z'-z''|$ we combine the integrals again. The integral over z'' can be evaluated analytically. To handle the divergence at $\mathrm{Im}\tilde{q}_\perp=0$ we introduce a cutoff L_z that corresponds to the vertical extension of the sample. Using the symmetry of the correlation function C_w in the variable Z we obtain

$$S(\mathbf{q})=\max\left\{L_z,\frac{1}{2\,\mathrm{Im}\tilde{q}_\perp}\right|$$
$$\left.\times\int d^3\mathrm{Re}^{-i\mathbf{q}_\parallel\cdot\mathbf{R}_\parallel}e^{-i\,\mathrm{Re}\tilde{q}_\perp Z}e^{-\mathrm{Im}\tilde{q}_\perp|Z|}C_w(\mathbf{R})\right., \tag{30}$$

with $\mathbf{R}=(\mathbf{R}_\parallel,Z)$. By the convolution theorem for Fourier integrals we get

$$S(\mathbf{q})=\max\left\{L_z,\frac{1}{2\,\mathrm{Im}\tilde{q}_\perp}\right\}$$
$$\times\int dp\hat{C}_w(\mathbf{q}_\parallel,p)\frac{1}{\pi}\frac{\mathrm{Im}\tilde{q}_\perp}{\mathrm{Im}\tilde{q}_\perp^2+(\mathrm{Re}\tilde{q}_\perp-p)^2}, \tag{31}$$

where $\hat{C}_w$ is the three-dimensional Fourier transform of the correlation function. The last term in the integral is the Fourier transform of $e^{-\mathrm{Im}\tilde{q}_\perp|Z|}$ and becomes the Dirac δ function for $\mathrm{Im}\tilde{q}_\perp\to0$. In this case the structure factor simplifies to

$$S(\mathbf{q})=L_z\hat{C}_w(\mathbf{q}_\parallel,\mathrm{Re}\tilde{q}_\perp). \tag{32}$$

We have $\mathrm{Im}\tilde{q}_\perp\neq0$ if either the medium is absorbing or $\theta_i<\theta_c$, respectively, $\theta_f<\theta_c$. The structure factor is then no longer simply the Fourier transform of the density correlation function but the convolution of the Fourier transform of C_w with a Lorentzian of full width at half maximum $2\,\mathrm{Im}\tilde{q}_\perp$. The convolution damps out oscillations of $\hat{C}_w$ in $\mathrm{Re}\tilde{q}_\perp$, which correspond to the vertical structure of the density fluctuations.

In the limit of strong absorption, vertical structures cannot be resolved any more. If the correlation length ξ of C_w is large compared to the scattering depth $\Lambda=1/|\mathrm{Im}\tilde{q}_\perp|$ (Ref. 4), then the z integration in (30) can be evaluated analytically after approximating $\hat{C}_w(\mathbf{q}_\parallel,Z)$ by $\hat{C}_w(\mathbf{q}_\parallel,0)$. This leads to the structure factor

$$S(\mathbf{q})=\frac{1}{|\tilde{q}_\perp|^2}\hat{C}_w(\mathbf{q}_\parallel), \tag{33}$$

which is identical to the one for the columnar model.

In the opposite case, for a correlation length ξ much smaller than the scattering depth, we make the approximation $e^{-\mathrm{Im}\tilde{q}_\perp|Z|}\approx1$ in (30) and get

$$S(\mathbf{q})=\tfrac{1}{2}\Lambda\hat{C}_w(|\mathbf{q}_\parallel|,\tilde{q}_\perp). \tag{34}$$

This is the same structure factor as derived for $\mathrm{Im}\tilde{q}_\perp=0$ in (32) with the cutoff L_z replaced by half the scattering depth.

To illustrate this effect we consider Poisson-distributed spherical single-particle scatterers of low density. Correspondingly, we substitute for $\hat{C}_w$ the Fourier transform of the correlation function of a sphere with radius R

$$\hat{C}_w(q)=\left[\frac{4\pi}{3}R^3\frac{\sin qR-qR\cos qR}{qR}\right]^2. \tag{35}$$

In the plots in Figs. 6 and 7 the radius equals $R=1000\lambda$ and the index of refraction $1-6.1\times10^{-6}+i\times10^{-7}$, as in the previous examples. Thus the critical angle is

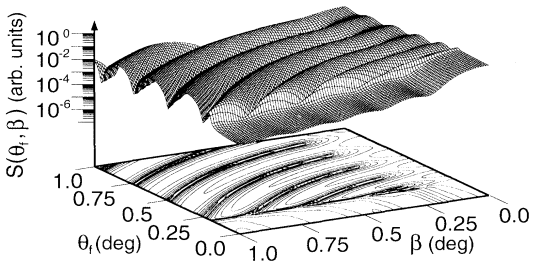

FIG. 6. A plot of the diffuse structure factor corresponding to the correlation function of a sphere with radius $R=1000\lambda$. The angle of incidence is $\theta_i=0.5°$ and the index of refraction $n=1-6.1\times10^{-6}+i\times10^{-7}$. The structure factor is plotted as a function of β and θ_f.

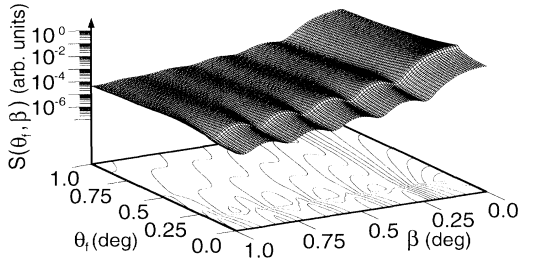

FIG. 7. The same as in Fig. 6 but at $\theta_i=0.1°$. The imaginary part of $\tilde{q}_\perp$ become big due to total external reflection.

$\theta_c=0.2°$. In Fig. 6 the structure factor is plotted as a function of θ_f and β at $\theta_i=0.5°>\theta_c$. For $\theta_f<\theta_c$ the imaginary part of $\tilde{q}_\perp$ suppresses any information about the vertical structure, and the intensity distribution resembles that of Fig. 5. In Fig. 7, θ_i is changed to 0.1° with the other parameters kept constant. Obviously, the vertical structure vanishes.

D. Layer model

In Sec. II B we discussed the specular reflectivity for density fluctuations restricted to a layer $a\le z\le b\le 0$ with the form (16) for w. We now consider the diffuse structure factor in this case. Correspondingly, we replace $C_w(\mathbf{R}_\parallel,Z)$ in Eq. (24) by

$$C_w(\mathbf{r}'-\mathbf{r}'')\Theta(z'-a)\Theta(b-z')\Theta(z''-a)\Theta(b-z'')\ , \tag{36}$$

with $C_w=C_w(|\mathbf{R}_\parallel|,|Z|)$, as in Sec. III C. Thus we obtain the structure factor

$$S(\mathbf{q})=\int d^2R_\parallel e^{-i\mathbf{q}_\parallel\cdot\mathbf{R}_\parallel}\int_a^b dz'\int_a^b dz'' e^{-i\,\mathrm{Re}\tilde{q}_\perp(z'-z'')+\mathrm{Im}\tilde{q}_\perp(z'+z'')}C_w(\mathbf{R}_\parallel,z'-z'')\ . \tag{37}$$

Substituting $Z=z'-z''$ and using the symmetry of C_w in Z the convolution theorem for Fourier transforms allows us to write

$$S(\mathbf{q})=\frac{1}{2\,\mathrm{Im}\tilde{q}_\perp}\int_{-\infty}^{\infty}dp\hat{C}_w(\mathbf{q}_\parallel,p)\frac{1}{\pi}\frac{\mathrm{Im}\tilde{q}_\perp}{\mathrm{Im}\tilde{q}_\perp^2+(\mathrm{Re}\tilde{q}_\perp-p)^2}2\{\cosh[\mathrm{Im}\tilde{q}_\perp(b-a)]-\cos[(\mathrm{Re}\tilde{q}_\perp-p)(b-a)]\}e^{\mathrm{Im}\tilde{q}_\perp(b+a)}\ . \tag{38}$$

As in Sec. III C, the Fourier transform of the correlation function appears in the structure factor in the form of a convolution integral. The result of Sec. III C for $\mathrm{Im}\tilde{q}_\perp\neq0$ is reproduced setting $b=0$ and $a=-\infty$ in Eq. (38).

In the case of columnar density fluctuations, i.e., C_w independent of z as in Sec. III B, the structure factor can be more easily calculated from (24) leading directly to

$$S(\mathbf{q})=\frac{1}{|\tilde{q}_\perp|^2}\hat{C}_w(\mathbf{q}_\parallel)e^{2\,\mathrm{Im}\tilde{q}_\perp b}\{1-2e^{-\mathrm{Im}\tilde{q}_\perp(b-a)}\cos[\mathrm{Re}\tilde{q}_\perp(b-a)]+e^{-2\,\mathrm{Im}\tilde{q}_\perp(b-a)}\}\ . \tag{39}$$

For $b=0$ and $a\to-\infty$ we recover the columnar model; compare with (28).

To provide an example for Eq. (39), we assume the same correlation function as in Secs. III A and III B. This describes a cylinder of length $b-a$ normal to the average surface. Radius, angle of incidence, and medium are chosen as in the examples of Secs. III A and III B, $R=1000\lambda$, $\theta_i=5.0°$, and $n=1-6.1\times10^{-6}+i\times10^{-7}$. Again, the structure factor is plotted as a function of θ_f and β. In Fig. 8, a layer from $b=-1000\lambda$ to $a=-1500\lambda$ is assumed. The thickness of 500λ corresponds to the minima of S at about $\theta_f\approx0.33°$ and $\theta_f\approx1.0°$. The decreasing scattering depth for $\theta_f<\theta_c$ causes a rapid decay of S for $\theta_f\to0$. For a layer beginning right at the surface, this effect is less dramatic, as

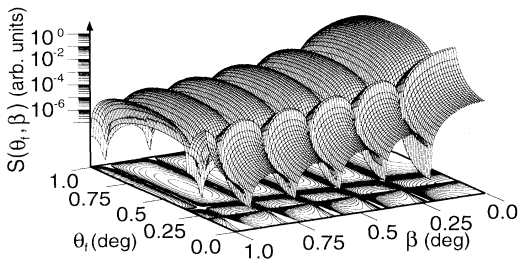

FIG. 8. The structure factor of density fluctuations restricted to a layer from $b=-1000\lambda$ to $a=-1500\lambda$ in a medium with $n=1-6.1\times10^{-6}+i\times10^{-7}$. The assumed correlation function and the angle of incidence are the same as in Figs. 4 and 5. The minima at $\theta_f\approx0.33°$ and 1.0° correspond to the layer thickness of 500λ.

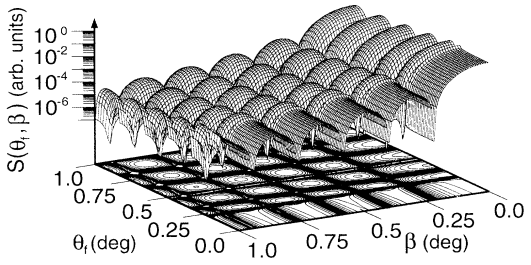

FIG. 9. The structure factor for the same correlation function as in Fig. 8, but for a layer from $b=0$ to $a=-2000\lambda$. The oscillations become shorter due to the greater layer thickness and the structure factor decreases more slowly for $\theta_f \to 0$ because the layer starts right at the surface. The angle of incidence is $\theta_i = 0.5°$.

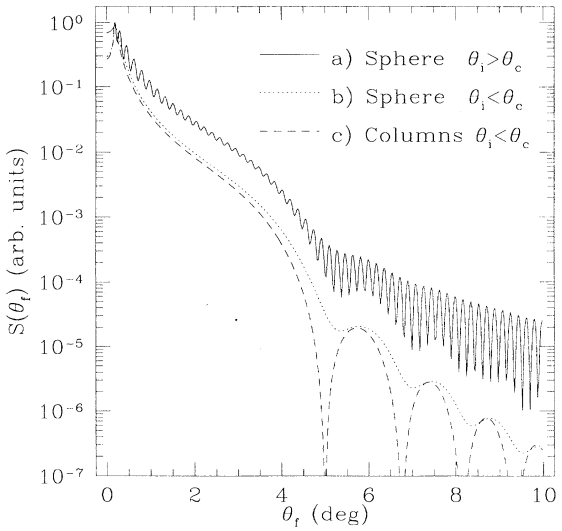

FIG. 10. The structure factor as a function of θ_f corresponding to the correlation function of a sphere with $R=1000\lambda$ at (a) $\theta_i > \theta_c$ and (b) $\theta_i < \theta_c$. For comparison the structure factor of columnar structures with the same radius is plotted in (c). All other parameters are equal to those of Figs. 6, 7, and 9.

shown in Fig. 9. There a layer from $b=0$ to $a=-2000\lambda$ is assumed. The greater thickness shows up in shorter oscillations in θ_f.

IV. CONCLUSIONS

In the preceding section we have discussed four cases with different restrictions on the geometry of density fluctuations. From the examples, we learn how to distinguish these geometries by studying the corresponding diffuse structure factor and the specularly reflected intensity. Layered structures can be characterized by the specular reflectivity which gives information about the layer thickness. The other three models discussed do not affect the specularly reflected intensity but can be distinguished only by the $\tilde{q}_\perp$ dependence of the diffuse scattering factor. δ-like density fluctuations have a structure factor that only depends on $\mathbf{q}_\parallel$, whereas for columnar structures the structure factor is proportional to $1/|\tilde{q}_\perp|^2$. The structure factor of isotropic density fluctuations has a more complex $\tilde{q}_\perp$ dependence which corresponds to the Fourier transform of the correlation function.

In contrast to conventional small-angle scattering, we had to take refraction effects into account. In the case of the angle of incidence and exit greater than θ_c, the imaginary part of $\tilde{q}_\perp$ is small and the main effect is a shift and a slight distortion of the diffraction pattern. If the angle either of incidence or of exit is below the critical angle so that $\mathrm{Im}\tilde{q}_\perp$ becomes large, the difference to ordinary small-angle scattering is considerable. First of all, the scattering signal becomes surface sensitive, as known from grazing incidence diffraction. Second, the large imaginary part and the small real part of the normal momentum transfer opens up the possibility to investigate lateral structures on length scales from nanometers up to some micrometers. These advantages become evident in two kinds of scattering geometries.

In the first one, θ_f is varied at constant $\theta_i < \theta_c$. In this case the dependence of $S(\mathbf{q})$ on $\mathrm{Re}\tilde{q}_\perp$ is smoothed out by the large $\mathrm{Im}\tilde{q}_\perp$ and one can take advantage of the enormous $\mathbf{q}_\parallel$ resolution of the θ_f scan.[2,3] This resolution is due to the slow variation of $\mathbf{q}_\parallel$ with θ_f, which allows us to measure the diffuse intensity at a large angular distance from the specular beam while still at very small $\mathbf{q}_\parallel$. In conventional small-angle scattering, e.g., at $\theta_i > \theta_c$, the vertical structure of the density fluctuations would dominate the θ_f dependence of the structure factor. Figure 10 illustrates this effect for the example of Sec. III C. Curves (a) and (b) show the structure factor for a θ_f scan for $\theta_i = 0.5°$ and $0.1°$, respectively. Whereas curve (a) shows short oscillations corresponding to the vertical extension of the sphere, the minima of curve (b) represent the pure $\mathbf{q}_\parallel$ dependence of $\hat{C}_w$. The typical length scale is in both cases equally $2R=2000\lambda$ and the structure factor for columnar structures with radius 1000λ plotted in curve (c) shows minima at approximately the same angles as curve (b).

In the second geometry, both angles $\theta_i, \theta_c < \theta_c$ and the diffuse intensity is measured as a function of β. This way, $\mathrm{Re}\tilde{q}_\perp$ is kept small while $\mathbf{q}_\parallel$ can be varied over a wide range. If $\theta_i \neq \theta_f$, we can again avoid the tails of the specular beam while measuring at small $\mathbf{q}_\parallel$ *and* $\tilde{q}_\perp$.

We would like to thank T. H. Metzger and J. Peisl for many enlightening discussions. Part of this work (T.S.) was supported by the Bundesministerium für Forschung und Technologie under Contract No. 055WMAX15.

[1]*Small Angle X-ray Scattering,* edited by O. Glatter and O. Kratky (Academic, New York, 1982).
[2]T. Salditt, H. Rhan, T. H. Metzger, J. Peisl, R. Schuster, and J. P. Kotthaus, Z. Phys. B **96**, 227 (1994).
[3]M. Tolan, G. König, L. Brügemann, W. Press, F. Brinkop, and J. P. Kotthaus, Europhys. Lett. **20**, 223 (1992).
[4]H. Dosch, *Critical Phenomena at Surfaces and Interfaces,* Springer Tracts in Modern Physics Vol. 126 (Springer, Berlin, 1992).
[5]R. Stömmer, J. Grenzer, J. Fischer, and U. Pietsch, J. Phys. D **28**, A216 (1995).
[6]A. Guinier and G. Fournet, *Small Angle X-ray Scattering* (Academic, New York, 1982).
[7]S. K. Sinha, E. B. Sirota, S. Garoff, and H. B. Stanley, Phys. Rev. B **38**, 2297 (1988).
[8]S. Dietrich and A. Haase, Phys. Rep. **260**, 1 (1995).
[9]J. M. Elson, Phys. Rev. B **30**, 5460 (1984).
[10]H.-G. Birken, Dissertation, University of Hamburg, 1991.
[11]W. Wu, J. Chem. Phys. **98**, 1687 (1993).
[12]V. Holý, J. Kuběna, I. Ohlídal, K. Lischka, and W. Plotz, Phys. Rev. B **47**, 15 896 (1993).
[13]V. Holý and T. Baumbach, Phys. Rev. B **49**, 10 668 (1994).
[14]D. K. G. de Boer, Phys. Rev. B **49**, 5817 (1994).
[15]A. Messiah, *Quantum Mechanics* (North-Holland, Amsterdam, 1961).
[16]L. Nevot and P. Croce, Rev. Phys. Appl. **15**, 761 (1980).
[17]A. Yoneda, Phys. Rev. **131**, 2010 (1963).
[18]L. S. Rodberg and R. M. Thaler, *Introduction to the Quantum Theory of Scattering* (Academic, New York, 1967).
[19]S. Flügge, *Mathematische Methoden in der Physik I, Analysis* (Springer, Berlin, 1979).
[20]D. G. Stearns, J. Appl. Phys. **65**, 491 (1989).

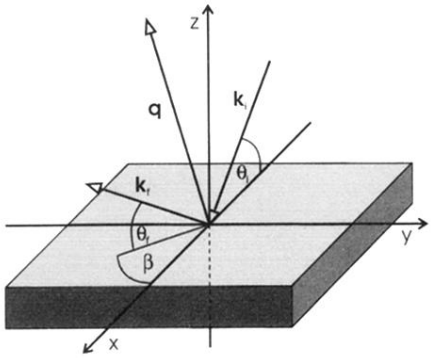

FIG. 1. Scattering of x rays under grazing incidence. The incident wave vector $\mathbf{k}_i$, the reflected wave vector $\mathbf{k}_f$, and the scattering vector $\mathbf{q}$ are illustrated. θ_i and θ_f are the angles of incidence and exit, respectively; β is the angle between the plane of incidence and the projection of the final wave vector on the surface.

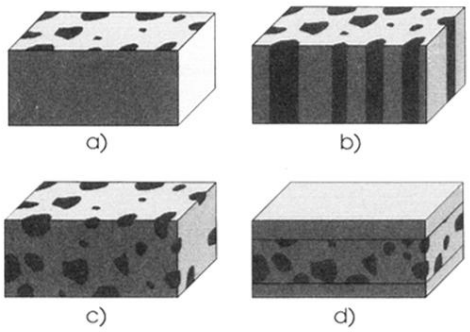

FIG. 3. Illustration of the four discussed restrictions on the geometry of the density fluctuations. A δ-like layer at the surface (a), columnar structures (b), isotropic density fluctuations (c), and a layered structure (d).